Appendix 2

Calculations of rate constants for the three-body recombination of H_2 in the presence of H_2

David W. Schwenke*
Eloret Institute, Palo Alto, CA 94303

Abstract:

We construct a new global potential energy hypersurface for $H_2 + H_2$ and perform quasiclassical trajectory calculations using the resonance complex theory and energy transfer mechanism to estimate the rate of three body recombination over the temperature range 100 - 5000 K. The new potential is a faithful representation of *ab initio* electronic structure calculations, is unchanged under the operation of exchanging H atoms, and reproduces the accurate H_3 potential as one H atom is pulled away. Included in the fitting procedure are geometries expected to be important when one H_2 is near or above the dissociation limit. The dynamics calculations explicitly include the motion of all four atoms and are performed efficiently using a vectorized variable-stepsize integrator. The predicted rate constants are approximately a factor of two smaller than experimental estimates over a broad temperature range.

---

* Mailing address: NASA Ames Research Center, Moffett Field, CA, 94035

I. Introduction

We have begun a detailed study of the calculation of recombination rate constants for hydrogen containing compounds in the gas phase. This is motivated by the need for these rate constants as input into modeling studies of hydrogen combustion processes. These processes in turn are important for the elucidation and design of a wide variety of hydrogen containing systems.

The initial system being considered is the recombination of hydrogen atoms to form H_2 in the presence of excess thermal H_2. This system has the advantage that it is one of the simplest possible and also there exist several experimental measurements which can be used to monitor the reliability of the theoretical predictions. The available experimental studies have been reviewed [1] and values for the recombination rate constants have been recommended over the temperature range 50-5000 K. The availability of experimental data will be important because the theoretical models used are not completely developed and the ultimate goal is to reliably predict rates for other systems or under conditions where experimental results are not available.

There have been several previous theoretical studies of gas phase recombination processes and different models and methods have been developed[2-6]. The particular model used in the present study was formulated by Roberts *et al.*[4] whereby the recombination rate is calculated from the rate of stabilization of quasibound resonant states by collisions with a third body. Of the available models, this resonance complex theory is the only one which takes into account the quantum mechanical nature of the metastable states involved in the recombination process. This model has been utilized in conjunction with the quasiclassical trajectory method to calculate recombination rates for hydrogen using several third bodies(H, H_2, He, and Ar in Ref.[7] and H in Ref.[8]). The present study closely follows this previous work but also includes several extensions and improvements.

The computational steps involved in the resonance complex theory are twofold. First of all, it is necessary to identify and characterize the important resonant states and secondly the rates of stabilization of these resonant states must be determined. For the present work we consider only the energy transfer mechanism in which case the resonant states are the metastable states of H_2. Previous workers have

2

well characterized these metastable states[9-11], thus in the present report we are concerned with the four body problem of collisions of thermal H_2 with metastable H_2.

The previous calculations for H_2 as a third body [7] made several approximations. Probably the most severe limitation was the use of empirical potential energy functions. Another possible source of error was the assumption that the thermal H_2 could be treated as a structureless particle. In the present work we eliminate these criticisms by constructing a new potential energy function which is based on *ab initio* electronic structure calculations and accurately treat the full four body dynamics. In addition, we use more accurate metastable state information and extend the results to higher temperatures.

The new potential is described and discussed in Sect. II, the dynamical methods are described in Sect. III, and our results are presented and discussed in Sect. IV. Finally in Sect. V we present the conclusions of this study.

All our calculations are carried out using hartree atomic units where the unit of energy is denoted E_h and 1 $E_h = 219474.7$ $cm^{-1} = 627.5095$ $kcal/mol = 4.3598$ $\times 10^{-18} J$, the unit of length is the bohr and is denoted a_o and 1 $a_o = 0.5291771$ $\times 10^{-10}$ m, the mass unit is the electron mass which is denoted m_e and 1 $m_e = 5.485804 \times 10^{-4}$ $a.m.u.$, and the time unit is equal to 2.418884×10^{-17} seconds.

II. Potentials

First consider the H_2 potential. The quasibound states of H_2 were studied for several potentials in Ref. [11] and because of the variation of the results seen there, it is desirable to employ the most accurate potential curve possible. The most accurate resonance parameters determined in Ref. [11] used a potential which included estimates of nonadiabatic effects. However this potential is not suitable for classical dynamics because it can not be represented as a single potential curve, thus instead we use the potential which includes all corrections except the nonadiabatic correction. The potential we will use is a representation of the one called Ad in Ref. [11]. This potential is based on the most accurate Born-Oppenheimer potential augmented by relativistic, radiative and nuclear motion corrections. The representation of the Ad potential used in Ref. [11] was a combination of a piecewise fifth order polynomial fit to the Born-Oppenheimer potential and its first derivative and cubic

spline representations of the various corrections to the Born-Oppenheimer potential. In addition, extrapolations using various functional forms for small and large bond length are involved when evaluating that potential. For the present calculations, it is desirable that the potential be represented in a form which avoids decisions in order to take full advantage of the vector processing capabilities available on class VI supercomputers. Thus we search for an alternate analytic representation.

We begin by writing the new ground state H_2 potential V_{HH} in the form

$$V_{HH} = V^{SR}(r) + V^{LR}(r), \qquad (1)$$

where r is the bond length, V^{SR} is a short ranged contribution and V^{LR} is the long range form of the potential, which is represented as

$$V^{LR} = -C_6/(r^6 + r_0^6) - C_8/(r^4 + r_0^4)^2 - C_{10}/(r^2 + r_0^2)^5. \qquad (2)$$

We take the dispersion parameters C_6, C_8, and C_{10} from previous calculations[12,13] and treat r_0 as an adjustable parameter. After some experimentation, we chose to represent V^{SR} as

$$V^{SR} = D\{exp[-\alpha(r)] - 1\}^2 - D, \qquad (3)$$

i.e. a Morse curve with a r dependent range parameter. Taking cognizance of the singularity at $r = 0$, we write

$$\alpha = r^{-s} \sum_{i=0}^{N} a_i r^i. \qquad (4)$$

The fitting procedure consists of first guessing values for r_0, s and N, then using Eqs. (1) and (2) to determine V^{SR}. The parameter D is then fixed by approximating α by $a(r - r_1)$ and determining D, a and r_1 so that V_{SR} is reproduced at the three values of r closest to the equilibrium separation of H_2. Once D is known, Eq. (3) can be inverted to give α at the input data points. The remaining parameters are then determined by linear least squares. This procedure is repeated as a function of r_0 in order to minimize the rms error produced in the fit to α. The data used in the fit are the values of the Ad potential from Ref. [11] evaluated at the distances where the Born-Oppenheimer potential was calculated[14].

4

An important problem for least squares fitting procedures is the method of weighting the various data points. For example, in the above procedure, an equally weighted least squares fit would tend to fit most accurately the values of α for large and small r since the magnitude of α is largest for these extremes. However, it is probably desirable to fit α most accurately for intermediate r, since that is where the wavefunction is likely to be largest. We accomplish this goal by using a weight function which is peaked in the vicinity of the equilibrium separation. The particular function used is the square of the ground state Morse oscillator wavefunction for the Morse parameters D, a, and r_1 determined above. In addition to these parameters a mass is required in the weight function - this parameter determines the width of the weight function. Empirically a value of 10 m_e was determined to be suitable.

In Fig. 1 the curves α and $r^s \alpha$ for $s=1$ are given. Both curves are very smooth and appear to be much easier to fit than the potential itself. The curve for $r\alpha$ looks approximately quadratic and so it might be expected that a low order fit would probably be quite adequate. However, because the potential for H_2 is known very accurately, it is necessary to use a high value of N to obtain satisfactory results. The final fit is obtained using $s=1$ and $N=16$ in Eq. (4). It should be noted that an important reason for the approximate linearity of α for large r is the separation of the long range and short range form of the potential. It would be interesting to see if these techniques would be useful for representing the potential of other diatomics.

An important problem when using high order polynomials is to make sure that they do not do strange things for bond lengths not included in the fit. This caused many trial fits to be rejected. The current fit to $r\alpha$ has only one zero for r real and $r \geq 0$ (the zero is near the equilibrium separation) and also $d[r\alpha]/dr$ has only one zero for r real and $r \geq 0$. The overall rms error of the fit is 2.78 mE_h, however the error decreases rapidly as r increases and the rms error for all points with $r \geq 1a_o$ is only $0.52 \mu E_h$. We have also computed the energy levels of all bound and quasibound states of H_2 using the WKB method for the current analytic representation and the original Ad potential and they agree very well. The rms difference is only 0.16 cm^{-1} while the maximum difference is only 0.30 cm^{-1}. Thus the current analytic representation satisfies our computational demands of no decisions for its evaluation without sacrificing accuracy. The parameters for this

5

representation are given in Table I. It should be noted that because the potential includes corrections to the Born-Oppenheimer potential which are mass dependent, it is only valid for the isotope of H with mass 1 $a.m.u.$

We now turn to the full H_4 potential. There have been several potentials proposed for the H_4 system, however few are applicable when one or more hydrogens are not at their equilibrium displacement and of these, fewer still are of documented accuracy when a hydrogen is stretched far from equilibrium. However, it is just these geometries which are expected to be important for the present application. Thus we will construct a new potential which concentrates on this aspect. The data we use to produce the new potential is the result of *ab initio* electronic structure calculations. There have been a large number of studies of the electronic structure of H_4, again mostly for hydrogen at its equilibrium separation. Because the classical equations of motion use as input only the gradient of the potential and not the potential itself, it will be important to accurately know the dependent of the potential on all degrees of freedom including bound length. Thus we perform new *ab initio* electronic structure calculations with these requirements in mind.

The electronic structure calculations where carried out using the MOLECULE-SWEDEN[15] codes with a gaussian basis set. The basis set consisted of 8 s functions contracted to 4 functions, 2 p functions and 1 d function per atom. The s function exponential parameters where taken from Ref. [16] and the contraction coefficients where determined from a calculation on the hydrogen atom. The p and d function exponential parameters where taken from Ref. [17]. The s components of the d functions were not included in the calculation giving a grand total of 60 contracted basis functions. With this atomic orbital basis, molecular orbitals where determined by performing a CASSCF calculation which included 4 orbitals in the active space. The energy produced by this calculation is denoted E^{CAS}. Using this molecular orbital basis, a multireference configuration interaction calculation was carried out including all single and double excitations out of the possible CAS reference configurations. The energy produced by this calculation is denoted E^{MRCI}. All calculations include all four H atoms to minimize problems of size consistency. With this basis set and correlation treatment, the difference in E^{MRCI} between two H_2 molecules with bond length 1.401 a_o separated by 20 a_o and four H atoms

no closer than 20 a_o to each other is $-0.345698\ E_h$, which is 99.1 % of twice the accurate value of the Born-Oppenheimer D_e.

Calculations were carried out for a total of 92 different geometries, all using C_{2v} symmetry, and the results are given in Tables II-VI. The number of geometries may seem low, but due to the high symmetry of this system and the method used to represent the potential energy hypersurface, these points should be sufficient for our purposes.

The *ab initio* electronic structure calculations we have carried out are expected to be accurate except in the vicinity of the Van der Waals minimum where much larger basis sets and more accurate correlation treatments are required[18]. This should not be a problem for two reasons. First of all it is possible to represent the potential in the vicinity of the Van der Waals minimum by using data describing the asymptotic form of the interaction potential, and secondly, the energies sampled by our dynamics calculations will be larger than the Van der Waals well depth, thus small to moderate errors there should not have a large effect on the calculated rate constants.

To represent the long range potential not given accurately by our electronic structure calculations, we will include a function in our analytic representation which has the proper asymptotic form. Most of the parameters of this function are determined not by the present electronic structure calculations but rather by other, more accurate, calculations. In particular the long range potential is represented as

$$V^{LR}_{AB+CD} = \sum_{q_1 q_2 \mu} v^{LR}_{q_1 q_2 \mu}(r_1, r_2, R) \mathcal{Y}_{q_1 q_2 \mu}(\theta_1, \theta_2, \phi), \qquad (5)$$

where $AB + CD$ denotes a particular way of drawing the bonds between four indistinguishable hydrogen atoms, r_1, r_2, R, θ_1, θ_2, ϕ_1, and ϕ_2 are the jacobi coordinates for $AB + CD$, and $\phi = \phi_1 - \phi_2$. The jacobi coordinates are defined so that r_i is the length of the vector $\vec{r}_i$ connecting the atoms in molecule i, R is the length of the vector $\vec{R}$ connecting the centers of mass of the two molecules, $cos\theta_i = \vec{r}_i \cdot \vec{R}/Rr_i$, and $cos\phi = (\vec{r}_1 \times \vec{R}) \cdot (\vec{r}_2 \times \vec{R})/|\vec{r}_1 \times \vec{R}||\vec{r}_2 \times \vec{R}|$. The angular functions are given by[19]

$$\mathcal{Y}_{q_1 q_2 \mu} = \frac{4\pi}{[2(1 + \delta_{\mu 0})]^{1/2}} [Y_{q_1 \mu}(\theta_1, \phi_1) Y_{q_2 -\mu}(\theta_2, \phi_2) + Y_{q_1 -\mu}(\theta_1, \phi_1) Y_{q_2 \mu}(\theta_2, \phi_2)],$$

$$(6)$$

where $Y_{q\mu}$ is a spherical harmonic. Because of homonuclear symmetry, only even values of the indicies q_1, and q_2 appear in Eq. (5). In Eq.(5), we will only include the terms with $q_1 + q_2 \leq 2$. The terms with $q_1 + q_2 < 2$ include dispersion and induction contributions and the terms with $q_1 + q_2 = 2$ also include the quadrapole-quadrapole interaction. We will include the dominant contributions for these terms and write

$$
v_{q_1 q_2 \mu}^{LR} = \begin{cases} -C_6^{q_1 q_2 \mu}(r_1, r_2)/[R^6 + d^{LR}(R)^6] \\ \quad -C_8^{q_1 q_2 \mu}(r_1, r_2)/\{[R^4 + d^{LR}(R)^4]^2\}, & q_1 + q_2 < 2; \\ \mathcal{Q}^{q_1 q_2 \mu} Q(r_1) Q(r_2)/[R^5 + d^{LR}(R)^5], & q_1 + q_2 = 2, \end{cases} \tag{7}
$$

where $C_6^{q_1 q_2 \mu}$ and $C_8^{q_1 q_2 \mu}$ are dispersion coefficients, d^{LR} is a damping function, Q is the quadrapole moment, and

$$
\mathcal{Q}^{q_1 q_2 \mu} = \begin{cases} 3/10, & \mu = 0; \\ \sqrt{2}/5, & \mu = 1; \\ \sqrt{2}/20, & \mu = 2. \end{cases} \tag{8}
$$

Everything except the damping function is obtainable from calculations by other workers. The damping function is determined by smoothly blending V_{AB+CD}^{LR} with the rest of the potential to approximately reproduce the Van der Waals minimum. In particular we use

$$
d^{LR} = d_1^{LR} exp(-d_2^{LR} R). \tag{9}
$$

For fitting purposes it is convenient to independently vary the quantities d_2^{LR} and $d^{LR}(R = 6.5\ a_o)$ rather than d_2^{LR} and d_1^{LR}. Then the parameter d_2^{LR} primarily controls the size of the long range potential for geometries which are mostly repulsive and $d^{LR}(R = 6.5\ a_o)$ controls the depth of the Van der Waals well.

The dependence of the quadrapole moment on bond length is parameterized by fitting the calculated values of Q from Ref. [20] over the range $r = 0.4$ to $4a_o$. We choose to represent it as

$$
Q = r^2(a_Q + b_Q r + c_Q r^2) exp[-(d_Q r)^2], \tag{10}
$$

with the parameters determined by equally weighted least squares. The parameters are given in Table VII. The rms error for this fit is $4.2 \times 10^{-3} a.u.$

8

The dependence of the dispersion parameters on bond length is not as well known, so it is necessary to resort to a more approximate procedure to parameterize this dependence. We do this by combining the values of the parameters for $r_1 = r_2 = 1.449a_o$ quoted in Ref. [21] along with the dispersion coefficients for $He + H_2$ from Ref. [18], which are given for three bond lengths. In particular, we write

$$C_n^{q_1 q_2 \mu} = [(2q_1 + 1)(2q_2 + 1)]^{-1/2} C_n^{q_1}(r_1) C_n^{q_2}(r_2) / \tilde{C}_n(He), \qquad (11)$$

where C_n^q is the dispersion coefficient for $He + H_2$ multiplying the Legendre polynomial of order q, and $\tilde{C}_n(He)$ is an effective dispersion coefficient for $He + He$ interactions, chosen so that equality holds in Eq. (11) when $r_1 = r_2 = 1.449a_o$. The square root factor in Eq. (11) arises because of the normalization factors of the spherical harmonics in the angular function $\mathcal{Y}_{q_1 q_2 \mu}$ not present in an Legendre polynomial expansion. The bond length dependence of the C_n^q is parameterized by writing

$$C_n^q = r^{m_n^q}(a_n^q + b_n^q r) exp[-(d_Q r)^2], \qquad (12)$$

i.e. we assume that the r dependence of C_n^q is similar to that of the quadrapole moment. The parameters for this equation are determined by equally weighted least squares. In Table VII we give the parameters for the functions $\tilde{C}_n^q$ which are the C_n^q rescaled so that the equation

$$C_n^{q_1 q_2 \mu} = \tilde{C}_n^{q_1}(r_1) \tilde{C}_n^{q_2}(r_2) \qquad (13)$$

is satisfied.

Equation (11) is an approximation, and it is interesting to estimate its accuracy by comparing the $\tilde{C}_n(He)$ to accurate values. For the case $n = 6$, we obtain values of $\tilde{C}_6(He)$ which range from 1.24 to 1.33 $a.u.$, while the accurate value is 1.47 ± 0.1 $a.u.$ [22], and for $n = 8$, 14.9 to 16.8 $a.u.$, as compared to 14.0 ± 0.2 $a.u.$ [22] Thus we see that Eq. (11) holds to about 20 %, which should be accurate enough for the present calculations.

We now turn to the representation of the repulsive part of the potential. One of the difficulties of producing an analytic representation for all atoms near together is the high symmetry in the H_4 system. This is especially true if the representation

needs to behave properly when H atoms are exchanged. When both molecules are near their equilibrium separation, it is convenient to expand the potential in terms of the jacobi coordinates r_1, r_2, R, θ_1, θ_2, and ϕ, as was done for the long range potential. However when R and the r_i become similar in size, it is not always clear how to drawn in the bonds, i.e. it may be ambiguous whether the system is best described by $AB + CD$, $AC + BD$ or $AD + BC$, where A-D are formally distinguishable H atoms. Thus a given set of jacobi coordinates are not suitable for a global representation of the potential. In the present situation we will handle this problem by first determining a representation for small vibrational displacements where the identity of the bonding and nonbonding pairs is clear, then switch to a more suitable representation for other configurations.

We begin our representation by extending the techniques of Ref. [23]. We first define the interaction potential to be the difference in energy between a geometry having particular values of r_1, r_2, R, θ_1, θ_2, ϕ and a geometry with the same values of r_1 and r_2 but with $R = 20\ a_o$. The total potential is the sum of the interaction potential and the bonding pair potentials, V_{HH}. The interaction potentials from the electronic structure calculations use E^{MRCI} and are denoted V^{MRCI}.

The first ingredient in the analytic representation is a nonbonding pairwise potential called V_P. This potential is determined by considering the interaction potential of the geometries having $\theta_1 = \theta_2 = \phi = \pi/2$. This is called the crossed geometry and its energies are given in Table VI. For these geometries, when both molecules have the same bond length, all of the nonbonding pairs are separated by equal distances, thus the nonbonding pairwise potential can be defined as one quarter of the interaction potential. To make this determination unique, only the eight geometries in Table VI having bond lengths equal to 1.401 a_o are used. This determines V_P only for eight distances, and we extrapolate and interpolate V_P by fitting it to the functional form

$$V_P = A_P exp(-B_P x^{C_P}), \tag{14}$$

with A_P, B_P, and C_P parameters. This fit is performed using nonlinear least squares with each point weighted by the amount $(|V^{MRCI}/4| + 10mE_h)^{-1}$, where V^{MRCI} is the interaction potential calculated from Table VI for that distance. Thus

10

the approximate relative error is minimized. The fit is quite good, giving as the minimized error 3.7×10^{-2} and an absolute rms error of 10 μE_h. The parameters for this fit are given in Table VII. It should be noted that V_P is positive everywhere. In Ref. [23], the nonbonding pairwise potential was generated at arbitrary distances by cubic spline interpolation, however we use Eq. (14) instead because of the smaller number of input data points and for the vectorization considerations mentioned above.

The nonbonding pairwise potential provides a reasonable zeroth order representation of the interaction potential, but it is not sufficiently accurate, so we make corrections to it. For small vibrational displacements, we write

$$V_{AB+CD}^{intSV} = [V_P(R_{AC}) + V_P(R_{AD}) + V_P(R_{BC}) + V_P(R_{BD})]F^c(r_1, r_2, R, \theta_1, \theta_2, \phi)$$
$$+ V_{AB+CD}^{LR}(r_1, r_2, R, \theta_1, \theta_2, \phi)$$

$$(15)$$

where V_{AB+CD}^{intSV} is the interaction potential for AB and CD close to their equilibrium displacements, R_{ij} is the distance between atom i and atom j, F^c is a multiplicative correction function, and V_{AB+CD}^{LR} is the long range potential defined above. In Ref. [23], a small factor was included to shift the potentials to ensure that F^c was always positive and always multiplied a positive function, however that is not required here because in the present case the long range attractive part of the potential is treated separately so that V_P and the differences between interaction potentials and the long range potentials included in the fitting procedure are automatically positive.

We now expand the function F^c as

$$F^c = \sum_{q_1 q_2 \mu} f_{q_1 q_2 \mu}^c(r_1, r_2, R) \mathcal{Y}_{q_1 q_2 \mu}(\theta_1, \theta_2, \phi), \qquad (16)$$

where the coefficients $f_{q_1 q_2 \mu}^c$ are to be determined and the angular functions are given by Eq. (6) above. To determine the $f_{q_1 q_2 \mu}^c$, we use the difference between the interaction potential and the long range potential for $r_i = 1.0$ or $1.401 a_o$, $R = 3.0$, 3.5, 4.0, 4.5, or 5.0 a_o, and $[\theta_1, \theta_2, \phi] = [0, 0, 0]$ (linear), $[\pi/2, 0, 0]$ (T shaped), $[0, \pi/2, 0]$ (T shaped), $[\pi/2, \pi/2, 0]$ (parallel) or $[\pi/2, \pi/2, \pi/2]$ (crossed), a total of 100 energies. This plus Eq. (15) gives F^c. The terms $(q_1, q_2, \mu) = (0,0,0)$, $(2,0,0)$, $(0,2,0)$, $(2,2,0)$, and $(2,2,2)$ are used in Eq. (16), and this equation is inverted to

11

give the $f^c_{q_1 q_2 \mu}$. The term $(q_1, q_2, \mu) = (2,2,1)$ is not included in the fitting procedure because it is zero for all the geometries for which we have calculated *ab initio* data. To generate the coefficients $f^c_{q_1 q_2 \mu}$ for arbitrary values of r_i and R, they are fit by linear least squares to the form

$$f^c_{q_1 q_2 \mu} = \sum_{i=0}^{1} \sum_{j=0}^{1} \sum_{k=0}^{1} c^{ijk}_{q_1 q_2 \mu} r_1^i r_2^j R^k. \tag{17}$$

All points are equally weighted in this fit and typically rms errors of about 0.3 mE_h are obtained. The final parameters $c^{ijk}_{q_1 q_2 \mu}$ are given in Table VIII.

It should be noted that the restriction of the angular functions in Eq. (16) to $q_1 + q_2 \leq 2$ does not imply a similar restriction on the potential V^{intSV}_{AB+CD} - the presence of the pairwise potential V_P ensures that higher order anisotropies exist.

The analytic representation of Eq. (15) works quite well when the bond lengths are not too large, but becomes less accurate for large displacements from equilibrium. For a typical example, see Fig. (2). We now define a large vibrational displacement potential which is more accurate for large bond lengths. A potential valid for both small and large displacements is obtained by smoothly switching from one to the other.

A subset of geometries where one bond length is very large is the situation where the system is most naturally described as $H_3 + H$, thus the large vibrational displacement potential will be forced to satisfy this limit. In particular, when one H is pulled away, the large vibrational displacement potential will reproduce a modification of the accurate LSTH H_3 potential[24]. The LSTH total potential is written in the form

$$V^{LSTH} = V^{Lon}_{H_3} + V^{NSB}_{HHH}, \tag{18}$$

where $V^{Lon}_{H_3}$ is obtained from the london equation:

$$V^{Lon}_{H_3} = \sum_{i=1}^{3} \mathcal{Q}_i - \{\frac{1}{2} \sum_{i>j} [J_i - J_j]^2\}^{1/2}, \tag{19}$$

where

$$\mathcal{Q}_i = \frac{1}{2}[^1 E(R_i) +^3 E(R_i)], \tag{20}$$

12

$$J_i = \frac{1}{2}[^1E(R_i) - {}^3E(R_i)], \tag{21}$$

R_i is one of the three interpair distances, ^1E is the H_2 singlet potential, ^3E is an effective H_2 triplet potential, and V_{HHH}^{NSB} is a correction function for nonsymmetric and bent geometries. Both $V_{H_3}^{Lon}$ and V_{HHH}^{NSB} are symmetric with respect to the interchange of any two H atoms. The simplest way to extend V^{LSTH} to H_4 is to write

$$V_{H_4}^{Lon} = \sum_{i=1}^{6} \mathcal{Q}_i - \{\frac{1}{2}[(J_1 + J_6 - J_2 - J_5)^2 + (J_2 + J_5 - J_3 - J_4)^2 + (J_3 + J_4 - J_1 - J_6)^2]\}^{1/2}, \tag{22}$$

where $\mathcal{Q}_i$ and J_i are defined by Eqs. (20) and (21) with interpair distances $R_1 = R_{AB}$, $R_2 = R_{AC}$, $R_3 = R_{AD}$, $R_4 = R_{BC}$, $R_5 = R_{BD}$, and $R_6 = R_{CD}$, and to write

$$V_{H_4}^{NSB} = V_{ABC}^{NSB} + V_{ABD}^{NSB} + V_{ACD}^{NSB} + V_{BCD}^{NSB}, \tag{23}$$

and

$$V_{H_4} = V_{H_4}^{Lon} + V_{H_4}^{NSB}. \tag{24}$$

In practice, this is modified in three ways. First of all, we replace the singlet function ^1E of Eqs. (20) and (21) with the H_2 potential V_{HH}. Secondly we slightly modify the effective triplet potential ^3E so that it is always greater than V_{HH} by writing

$$^3\tilde{E} = {}^3s(R)V_{HH}^{AM}(R) + {}^3E(R), \tag{25}$$

where

$$^3s = exp[-{}^3\alpha R^2], \tag{26}$$

and

$$V_{HH}^{AM} = D\{exp[-\alpha(R)] + 1\}^2 - D + V_{LR}(R), \tag{27}$$

D, α, and V_{LR} defined at the beginning of this section. The parameter $^3\alpha$ is given in Table VII and is determined to approximately minimize the effect of this change while ensuring the inequality $^3\tilde{E} > V^{HH}$. These two changes do not significantly alter the LSTH potential for geometries probed by most collisions. The final modification is to scale $V_{H_4}^{NSB}$ in Eq. (24) by a factor which goes to unity as the

13

configuration goes to $H_3 + H$. Thus the large vibration displacement total potential is

$$V^{LD} = \tilde{V}_{H_4}^{Lon} + S(\rho)V_{H_4}^{NSB}, \tag{28}$$

where $\tilde{V}_{H_4}^{Lon}$ is given by Eq. (22) with the replacements V_{HH} and $^3\tilde{E}$ for ^1E and ^3E in Eqs. (20) and (21), and the scaling function is given by

$$S = 1/\{1 + exp[-\beta(\rho - \rho_o)]\}, \tag{29}$$

where

$$\rho = (\sum_{i=1}^{6} R_i^2)^{1/2}. \tag{30}$$

The quantities β and ρ_o are parameters. The V^{LD} potential is symmetric with respect to the interchange of any two H atoms. The motivation of including the factor S can be seen in Fig. (2) where the interaction potentials derived from $\tilde{V}_{H_4}^{Lon}$, V_{H_4}, and V^{LD} are shown. In comparison to the ab $initio$ data, the $\tilde{V}_{H_4}^{Lon}$ potential is much too small and the V_{H_4} potential is much too large.

The small and large vibrational displacement potentials are now combined by defining the quantity

$$V_{AB+CD} = s^D(r_1+r_2)[V_{AB+CD}^{intSV} + V_{HH}(r_1) + V_{HH}(r_2)] + [1 - s^D(r_1+r_2)]V^{LD}, \tag{31}$$

where the switch s^D is given by

$$s^D = 1/\{1 + exp[a^D(r_1 + r_2 - r^D)]\}, \tag{32}$$

where a^D and r^D are parameters.

The final linear parameters in Eq. (17) are determined by approximately optimizing the nonlinear parameters β, ρ_o, a^D, d_2^{LR}, and $d^{LR}(R = 6.5\ a_o)$. The parameter r^D is fixed at a value of 5.4 a_o, which causes s^D to equal 1/2 when r_2 equals 4 a_o [see Fig. (2)]. The three nonlinear parameters β, ρ_o and a^D are adjusted to approximately minimize the weighted error in the interaction potential for all geometries having r_1 or r_2 greater than 2 a_o. The weight function used when r_1 or $r_2 > 2a_o$ is $(|V^{MRCI}| + 1mE_h)^{-1}$, where V^{MRCI} is the ab $initio$ interaction potential at these geometries. The parameters d_2^{LR} and $d^{LR}(R = 6.5\ a_o)$ are adjusted to

14

minimize the error in the points with r_i small and to produce good agreement with the potential expansion coefficients in the vicinity of the Van der Waals minimum given in Ref. [25]. The final parameters are given in Tables VII and VIII. The rms error for the fit to V_{AB+CD}^{intSV} is 0.29 mE_h and the weighted rms error for the points with r_1 or r_2 greater than 2 a_o is 1.8×10^{-3}.

The quality of the Van der Waals well can be estimated from Fig. (3). Here the first two functions $[(q_1,q_2,\mu) = (0,0,0), (2,0,0)]$ of an expansion like Eq. (5) of V_{AB+CD} is shown along with the data used to adjust the parameter $d^{LR}(R = 6.5\ a_o)$. The agreement is quite good. To be consistent with any systematic errors introduced in calculating the spherical average of the potential, we used the same method as in Ref. [25], namely that the interaction potential at the four geometries (linear, T-shaped, parallel, and crossed) and the difference between the interaction potential for a trapezoidal and parallelogram geometry is fit to a five term angular expansion. In addition, this figure shows the results of accurate calculations of the expansion functions. These were obtained by using converged numerical quadrature and the orthogonality of the $\mathcal{Y}_{q_1 q_2 \mu}$. The two methods of calculating the expansion functions do not differ greatly. Finally, this figure show the accurate expansion functions for the potential denoted DHR by Ref. [7]. These will be compared in detail in Sect. IV.

It should be noted that the angular expansion we use is different than that used in Ref. [25], however the two expansions are equivalent and are related by a nonsingular transformation.

In addition to the expansion functions, we have computed the geometry of the Van der Waals minimum and it has R=6.27, $r_1 = r_2 = 1.402\ a_o$, $\theta_1 = \pi/2$, $\theta_2 = \phi = 0$, and has a dissociation energy of 0.14 $kcal/mol$.

The remaining facet of the fit concerns the drawing of the bonds, i.e. whether the system is best described as $AB + CD$, $AC + BD$, or $AD + BC$. This ambiguity is resolved by defining a weight function for each of the three ways of drawing the bonds which picks out the appropriate way. To do this, define the quantity η_{AB+CD} as

$$\eta_{AB+CD} = [(r_1^{-2} + r_2^{-2})^{1/2} R]^{-1}, \tag{33}$$

where r_1, r_2 and R are a subset of the jacobi coordinates for drawing the bonds

as $AB + CD$. Of the three ways of drawing the bonds, the minimum value of η_{AB+CD}, η_{AC+BD} and η_{AD+BC} will likely indicate the most physical situation. The motivation for the functional form of Eq. (33) is as follows: in general the bonds should be drawn to minimize the individual bond lengths and maximize R. A differentiable expression for $min(r_1, r_2)$ is obtained by using $[r_1^{-n} + r_2^{-n}]^{-1/n}$ and taking the limit as n goes to ∞, however the simplest case of $n = 2$ seems adequate for the present application, thus η_{AB+CD} is approximately equal to $min(r_1, r_2)/R$. The motivation for maximizing R can be seen by considering a linear arrangement of the atoms in the order $ABCD$. If the atoms B and C were closer together than A and B or C and D, then a rule based only on $min(r_1, r_2)$ would select $AD + BC$ as the appropriate way to draw the bonds. However if the distance between A and B and the distance between C and D were equal, R for the arrangement $AD + BC$ would be zero. Thus maximizing R also would, for this example, select $AB + CD$ as the appropriate way to draw the bonds. Combining these ideas, we take the final potential to be

$$V = [S^A(\eta_{AB+CD})V_{AB+CD} + S^A(\eta_{AC+BD})V_{AC+BD} + S^A(\eta_{AD+BC})V_{AD+BC}]/$$
$$[S^A(\eta_{AB+CD}) + S^A(\eta_{AC+BD}) + S^A(\eta_{AD+BC})],$$

$$(34)$$

where

$$S^A(\eta) = exp[-\beta^A \eta], \qquad (35)$$

β^A a parameter we take to be 20. This final potential is symmetric with respect to interchanging any two H atoms.

An interesting quantity for a potential such as the current one which allows the possibility of hydrogen atom exchange, is what is the barrier for such an exchange. If the transition state for exchange is the square planer geometry, then the current potential predicts a barrier of 144 $kcal/mol$ with a side of length 2.7 a_o. This compares favorably with the *ab initio* value of 140 $kcal/mol$ at 2.4 a_o[26,27].

One unfortunate aspect of the present potential is that it is fairly time consuming to evaluate. In the trajectory calculations we require the gradient of the potential, and we calculate the gradient with respect to the six atom-atom distances and transform those derivatives using the chain rule to the form required by the equations of motion discussed below. The majority of the time spent evaluating

16

the gradient is spent determining the factor $\partial \phi / \partial R_{ij}$ for the three different sets of jacobi coordinates. These factors are required for any potential which is symmetric with respect to exchanging any two hydrogen atoms and has the correct long range quadrapole-quadrapole interaction. Thus there is nothing special about the present potential which makes it expensive to evaluate.

III. Dynamics Calculations

We follow Roberts *et al.*[4] and calculate the rate constant k^{3B} defined by
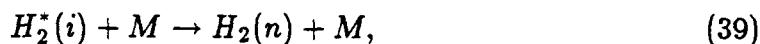
$$d[H_2]/dt = k^{3B}[H]^2[M], \tag{36}$$

for the process

$$H + H + M \rightarrow H_2 + M, \tag{37}$$

by modeling the recombination process as occurring via the steps

$$H + H \leftrightarrow H_2^*(i), \tag{38}$$

and

$$H_2^*(i) + M \rightarrow H_2(n) + M, \tag{39}$$

where M is thermal H_2, H_2^* is a quasibound state of H_2, i labels a particular quasibound state and n labels a particular bound state. This is the energy transfer mechanism. If the rate determining step is the process of Eq. (39) and the process of Eq. (38) is at equilibrium, then the rate constant can be written

$$k^{3B} = \sum_{i,n} K_{eq}^i(T) k_{in}^f(T) = \sum_i K_{eq}^i(T) \tilde{k}_i^f(T), \tag{40}$$

where K_{eq}^i is the equilibrium constant for Eq. (38), k_{in}^f is the rate constant for Eq. (39), $\tilde{k}_i^f$ is k_{in}^f summed over n, and T is the temperature.

If Eq. (38) for a particular quasibound state is not at equilibrium, then k^{3B} as calculated via Eq. (40) would be too large if that quasibound state was included in the sum. Thus we estimate nonequilibrium effects by simply neglecting all contributions to the overall rate due to that quasibound state[4]. Hence the quasibound states are partitioned into two groups, those that are approximately at equilibrium and those that are not. This is accomplished by computing the critical times [4] for

17

each quasibound state. The rate constants $\tilde{k}_i^f$ are required to calculate these critical times, however as the criterion for rejecting a particular critical time is approximate, we also approximate the rate constants by using hard sphere rate constants for the calculation of the critical times. These calculations are carried out for several temperatures and hard sphere parameters, and the net result is that quasibound states with resonance widths greater than about 0.001 cm^{-1} can be considered to be at equilibrium for the temperatures considered in the present study. Of the resonances characterized in Ref. [11], 38 can be considered to be at equilibrium (we use the resonance parameters calculated using the most accurate potential which includes estimates of nonadiabatic effects). In previous work [4,7,8], the list of quasibound states considered to be in equilibrium also included the $v = 14, J = 4$ state, however more accurate calculations [11] indicate that this state should be excluded. An additional restriction used previously [4,7,8] was to neglect quasibound states which have small equilibrium constants by virtue of their relatively high energies - this pared the list down to 6 quasibound states. However, because of the high temperatures considered here, we do not make this additional restriction.

The three-body recombination rate constant will be evaluated using the quasiclassical trajectory method. The third body M is taken to be thermal H_2, that is the rate constant k_{in}^f of Eq. (40) is given by

$$k_{in}^f = \sum_{m,m'} P_m(T)k_{im\to nm'}(T), \tag{41}$$

where m, m' are indicies labeling the bound states of H_2, P_m is the probability of being in state m at temperature T, and $k_{im\to nm'}$ is a state-to-state rate constant. The probability P_m is given by

$$P_m = \tilde{P}(J_m, \epsilon_m, T) / \sum_{m'} \tilde{P}(J_{m'}, \epsilon_{m'}, T), \tag{42}$$

where

$$\tilde{P} = g_J(2J + 1)exp(-\epsilon/\kappa T) \tag{43}$$

κ is Boltzmann's constant, and

$$g_J = \begin{cases} 1 & J \text{ odd}; \\ 3 & J \text{ even}. \end{cases} \tag{44}$$

18

The sum in Eq. (41) is accomplished by randomly selecting the initial state m with probability P_m as described in Ref. [28]. The states included in Eq. (41) are characterized using the WKB method and include only those having energies ϵ_m less than the dissociation energy. In particular, the energies ϵ_m are determined by searching for energies where the vibrational action J_v given by

$$J_v = \oint \{2\mu_{H_2}[\epsilon_m - V_{HH}(r) - (J_r^2/2\mu_{H_2}r^2)]\}^{1/2} dr \qquad (45)$$

is equal to

$$J_v = (v + 1/2)h, \qquad (46)$$

with v an integer. Above, μ_{H_2} is the reduced mass of H_2, and J_r is the classical rotational angular momentum and is given as

$$J_r = (J + 1/2)\hbar, \qquad (47)$$

J the quantum mechanical rotational angular momentum quantum number.

The sum in Eq. (40) will be evaluated in a similar manner to that used with Eq. (41). To do this, we write the equilibrium constant in the form

$$K_{eq}^i = N_{eq}(T)\bar{P}_i(T), \qquad (48)$$

where the probability $\bar{P}_i$ is given by

$$\bar{P}_i = \tilde{P}(J_i, \epsilon_i, T) / \sum_{i'} \tilde{P}(J_{i'}, \epsilon_{i'}, T), \qquad (49)$$

i and i' quasibound state indicies, and the factor N_{eq} is given by[4]

$$N_{eq} = (\frac{h}{\kappa \pi T m_H})^{3/2} 2^{-4} \sum_{i'} \tilde{P}(J_{i'}, \epsilon_{i'}, T), \qquad (50)$$

m_H the mass of an hydrogen atom. Then the recombination rate constant is given by

$$k^{3B} = N_{eq}(T) \sum_{i,m} \bar{P}_i(T) P_m(T) \sum_{n,m'} k_{im \to nm'}(T). \qquad (51)$$

Each trajectory is initiated by specifying a temperature T, a maximum impact parameter b_{max}, an initial separation d and by the choice of 12 random variables

19

$(\varsigma_1, ..., \varsigma_{12})$ uniformly distributed with $0 \leq \varsigma_i < 1$ and one random variable from a modified normal distribution. The first random variable ς_1 selects the initial state m using the probabilities P_m. This determines the internal energy and classical rotational angular momentum J_r for the bound H_2 molecule. The initial state of the quasibound H_2 is determined by ς_2 from the probabilities $\bar{P}_i$ - this determines the classical rotational angular momentum. The internal energy is fixed using a random variable selected from a modified normal distribution as discussed in detail below. Next the initial relative translational energy E_{rel} is set by finding the root of

$$\varsigma_3 = 1 - exp(-E_{rel}/\kappa T)(1 + E_{rel}/\kappa T), \tag{52}$$

which produces a Boltzmann distribution for E_{rel} [28]. The initial impact parameter b is then found from

$$b = b_{max}\varsigma_4^{1/2}. \tag{53}$$

From the masses, d, b, and E_{rel}, the initial cartesian coordinates and velocities of the centers of mass of the two H_2 molecules are fixed. The centers of mass are placed on the x axis, separated by d, and the initial velocities lie in the xz plane.

The initial coordinates and velocities of each diatom are determined by the random variables ς_5-ς_8 or ς_9-ς_{12}. First the initial bond length and its time derivative are determined as in Ref. [29] by numerically integrating the vibrational motion over the fraction ς_5 of the vibrational period. Next the orientation of the rotational angular momentum vector $\vec{\omega}$ is determined by the spherical polar angles $arccos[2(\varsigma_6 - 1/2)]$ and $2\pi\varsigma_7$. The magnitude of $\vec{\omega}$ is given by

$$\omega = J_r/\mu_{H_2}r^2. \tag{54}$$

Finally the rotational phase is specified by ς_8. With this information the cartesian coordinates and velocities of the atoms with respect to the center of mass of the diatom are fixed. The same procedure is then used with ς_6-ς_{12} for the second molecule. This information, combined with the position and velocities of the centers of mass, completely specifies the initial conditions of the four atoms.

We next discuss in detail our selection of the initial internal energies of the quasibound states. For the evaluation of the probabilities $\bar{P}_i$, we will use the energies from the most accurate potential of Ref. [11], which includes estimates of

nonadiabatic effects. The use of the accurate energies presents a problem for some of the quasibound states, because sometimes the resonance energies lie above the centrifugal barrier, thus these states are not classically bound. In the previous studies, this problem was avoided by modifying the diatom potential[7] or by arbitrarily decreasing the energy[8] so that these states became classically bound. Here another approach is taken. We interpret the quasibound states as states with uncertain energies. In particular, rather than ascribing the energy ϵ_i to all quasibound states labeled by i, the energies are chosen randomly from a probability distribution peaked about ϵ_i. The distribution used is a modified normal distribution given by

$$P(\epsilon)d\epsilon = \begin{cases} 0, & \epsilon > V_{J_i} - \delta; \\ 0, & \epsilon < \delta; \\ N_i exp[-(\frac{\epsilon-\epsilon_i}{4\Gamma_i})^2], & \text{otherwise,} \end{cases} \tag{55}$$

where V_J is the height of the centrifugal maximum for angular momentum J, δ is a small number taken to be $4\mu E_h$, N_i is a normalization constant, and Γ_i is the resonance width for quasibound state i. The energies generated by this distribution are calculated using the rejection method using the unmodified normal distribution as the comparison function[30].

All uniformly distributed random numbers were generated by shuffling a multiplicative congruential quasirandom number sequence. The shuffling was performed using algorithm B of Ref. [31] using the parameter $k = 99$, and the parameters used for the multiplicative congruential generator were modulus 2^{64} and multiplier 6364136223846793005 [31]. The reasons for using this random number generator are twofold. First of all it is machine independent so that calculations performed on different computers can easily use the same random number sequences, which is useful for comparing results. Secondly, and more importantly, it is a much higher quality random number generator than is typically available from operating system libraries. In the present application where we are performing monte carlo integration of high dimensionality, it is probably important that high quality random numbers are used.

The final state analysis is the same as used previously[7], namely diatoms with energies less than the dissociation energy are considered bound and all others are not. We will use stratified sampling[29] for calculating the final rate constants, i.e.

different trajectories for a given T will have different values of b_{max}. We use two values of b_{max}, called b_1 and b_2. Then if N_i is the total number of trajectories for a given temperature and N_i^{bound} is the number of trajectories which resulted in two bound H_2 molecules when $b_{i-1} < b \le b_i$ (b_0 is zero), then the recombination rate constant is given by the expression

$$k^{3B} = N_{eq}(T)(\frac{8\kappa T}{\pi \mu_{H_2+H_2}})^{1/2} \pi \sum_i (b_i^2 - b_{i-1}^2) N_i^{bound}/N_i, \qquad (56)$$

$\mu_{H_2+H_2}$ the reduced mass for $H_2 + H_2$ collisions. The one sigma error associated with this quantity is

$$\Delta k^{3B} = N_{eq}(T)(\frac{8\kappa T}{\pi \mu_{H_2+H_2}})^{1/2} \pi [\sum_i (b_i^2 - b_{i-1}^2) N_i^{bound}(N_i - N_i^{bound})/N_i(N_i-1)]^{1/2}. \qquad (57)$$

The actual integration of the trajectories will be now discussed. The integration coordinates used are a generalization of those used in Ref. [32], namely we initially require that the center of mass of the system be stationary at the origin of our cartesian coordinate system - then the motion of the four atoms with respect to the center of mass is determined by 9 cartesian coordinates and their conjugate momenta. We use as the 9 cartesian coordinates the coordinates of the first three atoms.

In general if there are N atoms, and the center of mass is stationary at the origin, we can use as independent coordinates the cartesian coordinates of the first $N-1$ atoms. If these coordinates are denoted by the column vector $\mathbf{q}$ with elements $(x_1, y_1, z_1, x_2, ..., z_{N-1})$ for atoms $1, 2, ..., N-1$, then the kinetic energy E_{kin} can be written

$$E_{kin} = \frac{1}{2}\dot{\mathbf{q}}^T M \dot{\mathbf{q}}, \qquad (58)$$

where $\cdot$ denotes time derivative, T transpose, and the matrix M has elements defined by

$$\mathbf{M}_{ij} = \begin{cases} m_k + m_k^2/m_N, & i = j = 3(k-1) + l, l = 1, 2, \text{ or } 3; \\ m_k m_p/m_N, & i = 3(k-1) + l, j = 3(p-1) + l, l = 1, 2, \text{ or } 3; \\ 0 & \text{otherwise.} \end{cases} \qquad (59)$$

The Hamiltonian is then given by [33]

$$H = \frac{1}{2}\mathbf{p}^T M^{-1} \mathbf{p} + V, \qquad (60)$$

22

where V is the potential energy and the conjugate momenta p are given by

$$\mathbf{p} = \mathbf{M}\dot{\mathbf{q}}. \tag{61}$$

Hamilton's equations of motion are then

$$dq_i/dt = \sum_j p_j (\mathbf{M}^{-1})_{ji} \tag{62}$$

and

$$dp_i/dt = -\partial V/\partial q_i. \tag{63}$$

We have considered two numerical methods for integrating Eqs. (62) and (63). Originally we used the fourth order Adams-Bashforth-Moulton predictor-corrector algorithm, with fixed time steps[34], which is a common integrator used for classical trajectories [28]. However as pointed out previously [7], it is necessary to take very small time steps to obtain accurate results because at certain times the atoms can have very high velocities. This happens when a diatom is near its equilibrium separation when its kinetic energy can be close to the bond energy of H_2. However most of the time, the atoms will be moving much slower, thus much computational effort is wasted using a fixed stepsize integrator. For this reason we seek an efficient variable stepsize integrator.

The results of tests of several different integrators for classical trajectories was reported in Ref. [28], and the one we have chosen to develop is the Burlisch-Stoer method [34,35]. This method is recommended in Refs. [28,34] over several other methods. An important advantage which will be exploited here is that variable time steps can be used and programmed in a manner which does not have a detrimental effect on the efficient use of the vector capabilities of modern supercomputers. This method and our modifications to it are now described in detail.

In the Burlish-Stoer method, in order to integrate the differential equations over some time increment H, one performs several calculations using a low order method (the modified midpoint rule) which differ in the time steps used. The time steps are from the special pattern $h = (H/2, H/4, H/6, H/8, H/12, ...)$, and the results are extrapolated to zero stepsize using a rational function. No information from previous steps is required for the current step, thus the method is self starting,

23

unlike the Adams-Bashforth-Moulton method, and also the time increment can be changed at will. It should be noted that the time interval H is typically much larger than the stepsizes used by other integrators, thus this method is not a good one if the solution of the differential equation is required on a fine time grid.

In the implementation of integrating a single set of coupled differential equations, it is typical to extrapolate the results after each modified midpoint calculation, and continue decreasing the time step until the extrapolation converges. Then the time interval H is adjusted so that the expected number of integrations required for convergence at the next time step will be some predetermined optimum number[34]. However in the present application, we will take advantage of vector processing by simultaneously integrating a number of independent trajectories, thus it will not be efficient to keep decreasing the time step until the trajectory which is most difficult to integrate is converged. Thus we modify the above scheme by integrating all trajectories using a predetermined number of stepsizes. Each trajectory will have its own time increment. After the integrations over a time increment are carried out, the errors in the extrapolations from the various stepsizes are checked. If the errors are small enough, the time interval H for that trajectory is increased and the clock is advanced. If the errors are too large, the results from the time increment are thrown away, H is reduced and the clock is not advanced. Occasionally the trajectories are checked for completion, and if required, finished trajectories are removed and new ones are started. This scheme is vectorizable except where the time increment H is changed and end tests are performed, but these steps usually amount to an insignificant portion of the total resources required in a calculation, thus this algorithm runs efficiently on vector pipeline supercomputers.

We now discuss some details of the algorithm, in particular how the errors are estimated and the time interval is changed. Let the number of different time steps per time interval H be N^{TS} and define the quantity $\xi_j^{(i)}$ to be the j'th integration function (one of the $6N - 6$ coordinates and conjugate momenta) resulting from the i'th extrapolation using the first i time steps. We estimate the errors of the extrapolations to be

$$\Delta \tilde{\xi}_j^{(i)} = |\xi_j^{(i)} - \xi_j^{(N^{TS})}|, \ i = 1, ..., N^{TS} - 1. \tag{64}$$

To remove the units in this error and to smooth out the variations from trajectory to trajectory, this error is scaled by the rms initial value of either all coordinates or all momenta for this trajectory - this produces a relative error called $\Delta\xi_j^{(i)}$. Finally the maximum error over all j is called $\Delta^{(i)}$ and this is used to characterize the error obtained using i time steps. This error is compared to an error tolerance parameter ϵ, and the largest value of i for which $\Delta^{(i)}$ is greater than ϵ is determined - this value of i is called $i^C - 1$. If all $\Delta^{(i)}$ are greater than or equal to ϵ, then the error is unacceptably large and the time increment H is reduced by a factor of $1/N_{N^{TS}/2}^{Step}$, where N_i^{Step} is the ratio of the time increment H to the time step h for integration i. If i^C is less than N^{TS}, then the time increment is increased by the factor $[(N_{N^{TS}}^{Step}/N_{i^C+1}^{Step}) + w]/(1 + w)$, where w is a fixed damping parameter which we usually take equal to $1/2$.

In practice, this time increment changing algorithm works quite well - see Fig. (4) where the relative error versus CPU time is compared for the current method and the Adams-Bashforth-Moulton method. For the present application the Burlisch-Stoer method is always more efficient then the Adams method, and its superiority increases rapidly as the desired relative error decreases. Thus there is less motivation to scrimp using the present method, for a small increase in CPU time can produce a large increase in accuracy. The data for this figure is based on calculations with N^{TS} equal to 5, w equal to $1/2$, which experiments show to be about optimum for the present application. In general larger values of N^{TS} allow larger time increments but if the time increment becomes too large, the terrain covered in a single increment will be sufficiently varied so that it is not possible to make significant adjustments to the time increment. This tends to favor smaller values of N^{TS} for the present application. Initial conditions for the trajectories were selected as described above for a temperature of 5000 K, b_{max} equal to 8 a_o, and an initial separation d equal to 15 a_o. The potential $\tilde{V}_{H_4}^{Lon}$ was use for these calculations. Ten trajectories were integrated forward for a time of 8000 $a.u.$, then back integrated for a time 8000 $a.u.$ The times reported as the abscissa are the average CPU seconds for each trajectory using a single CPU on the Ames ACF Cray-XMP/48. Since these were obtained running only ten trajectories and did not use the accurate potential, they are not indicative of the times required for

25

our production calculations. We estimate that our production calculations require about a factor of five less time under these conditions. The relative error reported is the rms relative difference between all of the initial position and momentum variables and their back integrated values. The value of 8000 $a.u.$ is a typical integration time for the conditions used here. The initial value of H was take to be 10 $a.u.$ for all calculations of Fig. (4). As an example of the changes made to H, when ϵ was 1×10^{-5}, H ranged from 7.6 to 87.7 $a.u.$, an average of 195 successful and 23 unsuccessful time increment steps were taken per trajectory and the rms relative error was 6.2×10^{-4}. Another advantage of a variable stepsize integrator is that the errors for each trajectory are about the same - when the rms relative error was 6.2×10^{-4}, the rms relative errors for individual trajectories varied by a factor of 53, while when using the Adams-Bashforth-Moulton method with a stepsize giving a similar rms relative error of 1.9×10^{-4}, the rms relative errors for individual trajectories varied by a factor of 3200.

Although the increment changing algorithm works well, it suffers from several potential drawbacks. First consider the determination of the error $\Delta \xi_j^{(i)}$. As presently described, if one were to change the initial separation between the molecules, but nothing else, the integrator would allow larger errors because the scaling factor, which is based on the rms initial conditions, would be increased. Another manifestation of this is that trajectories with larger initial impact parameters would be allowed to have larger errors. An additional question is what the relative weighting of the errors in the coordinates and the momenta should be for optimum performance. Turning to the time increment changing algorithm, it always tries to increase the time increment until it is too big and a step is rejected. It would be better to have some method of slowly decreasing the time increment as the errors get larger, however this would increase the complexity of the algorithm. Once it has been decided to increase the time increment, the factor we use to increase it is somewhat arbitrary, and situations may arise where increasing the time increment by $N_{NTS}^{Step}/N_{i^C+1}^{Step}$ would lead to a excessively large increment. The inclusion of the damping parameter w is an attempt to forestall this possibility of increasing the time increment too quickly and then having to decrease it right away. The time increment decrease factor is also arbitrary, however it seems to satisfy two important

properties, namely that it is unlikely that two decreases occur consecutively and that the increase algorithm can overcome the rapid decrease in a few applications, if the error is small enough.

An additional aspect of the present calculations concerns the question of the number of trajectories to be integrated simultaneously. The larger the number, the more efficient the calculations will be since we use vector pipeline supercomputers (various calculations were performed the the Ames ACF Cyber 205, Cray-XMP/48, or the NAS facility Cray-2). On the other hand, larger numbers require more computational resources. For most production calculations, we integrate a maximum of 500 trajectories simultaneously. This number is large enough so that significant additional speedups are not possible by increasing it further.

IV. Results and Discussion

The main results of this paper are given in Table IX. The rate constants for each temperature are based on the results of 4000 trajectories which produces statistical one sigma errors of about 5 %. All calculations use an initial separation d equal to 15 a_o and were terminated when any atom-atom distance exceeded 27 a_o. The maximum impact parameters (b_1, b_2) varied from (6.4,8) a_o at 5000 K to (8.4,12) a_o at 100 K. Most calculations used the integration parameters N^{TS}=5, $w = 1/2$, $\epsilon = 1 \times 10^{-5}$, and a initial time increment of 10 $a.u.$ The remaining calculations used an earlier version of the error control algorithm and should produce results of commensurate accuracy.

At low temperatures, no exchange processes occurred and so it was probably not necessary to force the potential to be symmetric with respect to exchanging atoms, but at higher temperatures this symmetry is more important. For 2000 K, 0.13 % of the trajectories ended up in other than the initial arrangement $AB + CD$, at 3000 K the number was 1.0 % and at 5000 K, 3.7 %. Also it is not known how many trajectories crossed only temporarily into other arrangements, thus it is probably good that our potential is symmetric. The 144 $kcal/mol$ barrier to exchange may seem too large to allow any exchange reactions, but the quasibound states have at least 109 $kcal/mol$ of energy making the effective barrier no more than 35 $kcal/mol$. Thus the exchange rates we observe are not unreasonable.

In addition to Table IX, our results are also shown in Fig. 5 along with several

27

experimental measurements of the recombination rate constants[1,36-41]. We show the results of the measurements of one laboratory for a range of low temperatures where the measurements of various groups agree fairly well, and the results of several groups at high temperature to show the spread obtained there. At 100 K, the theoretical results are too small by a factor of about 3, and at the higher temperatures, the theoretical results are about half of the recommended values. The temperature dependence of the present results are similar to estimates of the experimental temperature dependence, however they tend to fall off too quickly at low temperature ($T < 200\ K$). For high temperature, the theoretical results also appear to fall off too quickly, however the situation is less clear because of the uncertainty in the experimental measurements. In analyzing the experiments, it is common to assume that $k^{3B} = A/T^m$ [36-38,40], and some in experiments, there is insufficient information to accurately determine the exponent m so a value of one is assumed [36-38]. Thus the experimental temperature dependence is not well determined over the range 3000-5000 K.

Because of the relatively poor agreement with experiment, it is interesting to compare to the results of previous calculations. The two temperatures in common are 100 and 300 K where we obtain 1.84 $\times 10^{15}\ cm^6\ mol^{-2}\ sec^{-1}$ and 1.52 $\times 10^{15}$, Whitlock et al.[7] obtain 6.6 $\times 10^{15}$ and 4.2 $\times 10^{15}$ using their DHR potential, and experiment gives 6.2$\pm$0.7 $\times\ 10^{15}$ (this is estimated from the graph of Ref. [41]) and 3.0$\pm$0.2 $\times\ 10^{15}$ (at 298 K [41]). The results of Whitlock et al. [7] are in better agreement with experiment than our presumably more accurate calculations. A detailed analysis shows that the differences between the two calculations are primarily due to a combination of the differences in the interaction potential and the differences in the diatomic potential. If we repeat our calculations using the DHR potential of Ref. [7] instead of the ab initio interaction potential of Sect. II (we use our accurate diatomic potential), we obtain 4.09 $\times 10^{15}$ and 2.73 $\times 10^{15}$. The 300 K results of this calculation are in even better agreement with experiment and further calculations using the DHR potential at higher temperatures continue this trend [see Fig. (6)].

We may then ask if the DHR potential is more accurate than the ab initio potential since it produces results which are in closer agreement with experiment.

28

If this were so, it would be quite surprising for the DHR potential is very simple, comprising of the sum of pairwise interactions. It is not easy to pin point the features of the potentials primarily responsible for the differences in the dynamics, however it is possible to single out two differences. First of all consider Fig. (2) where the dependence of the interaction potential on bond length is shown. The *ab initio* calculations clearly indicate that for bond lengths near equilibrium, the potential increases as the bond length increases and as the bond length becomes larger, this trend reverses. In contrast, for the geometry of this figure, any pairwise potential, including the DHR potential, will cause the potential to monotonically decrease as the bond length increases. This difference in force should have a profound effect when both molecules are near their equilibrium displacement[42]. Next consider the anisotropies of the two potentials. These are also very different when both molecules are near their equilibrium separation - this is shown in Fig. (3). For R less than 5 a_o, the DHR potential gives a leading anisotropy which is an order of magnitude larger than the *ab initio* potential. The spherical average of the DHR potential agrees well with the *ab initio* potential. The differences in the anisotropies should have a big effect on rotational energy transfer. It is beyond the realm of possibility that the *ab initio* calculations have errors so large that the DHR potential is the accurate potential for the features just discussed, however these features are not necessary the primary progenitors of the differences in the dynamics calculations. However, it is most likely that the *ab initio* potential is much more globally accurate than the DHR potential and that the good agreement with experiment obtained using the DHR potential is due to fortuitous cancellations of error.

There are several possible reasons why the present calculations underestimate experiment by such a large factor. First of all there are errors in the present results because of the use of an approximate potential energy function. However preliminary results obtained on different potentials based on the *ab initio* calculations were quite similar to the present results and so it seems unlikely that reasonable variations in the potential alone could make up for the difference. Another fault of our calculations is that they use classical dynamics. Classical dynamics has not been tested for a system such as this one, however one usually expects reasonable accuracy for calculations involving highly excited states, such as those involved in

29

the present study. On the other hand, classical dynamics is unreliable for describing processes for which tunneling plays an important role. Thus the present use of classical dynamics must be treated with some suspicion because of the presence of hydrogen atoms which can undergo large amounts of tunneling. In addition, tunneling plays an important role in the formation and decay of the quasibound states.

Furthermore, several processes are omitted from the present calculations, namely the possibility of direct association from the continuum as well as contributions to the recombination rate from other processes involving quasibound states, e.g. the chaperon mechanism:

$$H + H_2 \leftrightarrow H_3^*, \tag{65}$$

$$H + H_3^- \rightarrow 2H_2. \tag{66}$$

Estimates from Ref. (4) indicate that direct association from the nonresonant continuum relative to the association from the quasibound states will become more important as the temperature increases, however if this was the main cause for the underestimate, then one would expect that the present results would underestimate experiment by increasing amounts as the temperature increases. This contrasts to the approximately constant underestimate of a factor of two over a fairly broad temperature range, thus it seems unlikely that the neglect of direct association is the primary fault of the present calculations. As far as the chaperon mechanism is concerned, it seems to be important only at lower energies than we consider here [5-7]. However, this mechanism may be responsible for the underestimate at low temperatures [see Figs. (5)-(6)]. It should be noted that a converged quantum mechanical dynamics calculation would properly take into account the role of the continuum and the chaperon mechanism

Finally one can consider the possibility that the resonance complex mechanism is not the proper route for calculating the recombination rate constants - this is because the bottleneck for the association may occur elsewhere when nonequilibrium and redissociation processes are considered. In particular Ashton et al.[43] conclude from their model calculations that the primary bottleneck occurs in the relaxation of bound vibrational states close to the dissociation limit. Thus the results of

the resonance complex mechanism should be an upper bound to the true rate of recombination which then means that the underestimate of the present calculations is even greater than indicated in Fig. (5).

There exists one more possibility for explaining the underestimate, namely that the experimental results are systematically high. However this seems unlikely due to the degree of agreement between various experimental workers and we will not consider this as an serious proposition until the approximations in the current theoretical work have been more thoroughly tested.

V. Conclusions

We have carried out calculations of the recombination rate constants for the process $H + H + H_2 \rightarrow 2H_2$ using a quasiclassical trajectory implementation of the energy transfer mechanism of the resonance complex theory. A new global potential energy function for H_4 is constructed which should be accurate for geometries important to the dynamics calculations. In spite of the quality of these inputs into the calculation, the agreement with experimental results is not very good with the theoretical results about a factor of 2 too small over the temperature range 300 - 5000 K. Of the are several possible causes for this underestimate, the most likely reason is the importance of quantum effects. This and other limitations must be studied in order to predict with confidence three body recombination rate constants for hydrogen containing compounds.

VI. Acknowlegdements

References:

1. N. Cohen and K. R. Westberg, J. Phys. Chem. Ref. Data **12**, 531 (1983).

2. D. L. Bunker, J. Chem. Phys. **32**, 1001 (1960).

3. J. C. Keck, J. Chem. Phys. **32**, 1035 (1960).

4. R. E. Roberts, R. B. Bernstein, and C. F. Curtiss, J. Chem. Phys. **50**, 5163 (1969).

5. V. H. Shui and J. P. Appleton, J. Chem. Phys. **55**, 3126 (1971).

6. R. T Pack, R. L. Snow, and W. D. Smith, J. Chem. Phys. **56**, 926 (1972).

7. P. A. Whitlock, J. T. Muckerman, and R. E. Roberts, Chem. Phys. Lett. **16**, 460 (1972); J. Chem. Phys. **60**, 3658 (1974).

8. A. E. Orel, J. Chem. Phys. **87**, 314 (1987).

9. R. J. LeRoy and R. B. Bernstein, J. Chem. Phys. **54**, 5114 (1971).

10. C. Schwartz and R. J. LeRoy, J. Mol. Spect. **121**, 420 (1987); R. J. LeRoy and C. Schwartz, University of Waterloo Chemical Physics Research Report CP-301 (1986).

11. D. W. Schwenke, Theor. Chim. Acta, submitted.

12. W. Kołos, Int. J. Quan. Chem. **1**, 169 (1967).

13. W. J. Deal and R. H. Young, Mol. Phys. **19**, 427 (1970).

14. W. Kołos, K. Szalewicz, and H. J. Monkhorst, J. Chem. Phys. **84**, 3278 (1986).

15. MOLECULE is a vectorized gaussian integral code written by J. Almlöf and SWEDEN is a vectorized SCF-MCSCF-direct CI -conventional CI-CPF-MCPF program written by P. E. M. Siegbahn, C. W. Bauschlicher, B. Roos, P. R. Taylor, A. Heiberg, J. Almlöf, S. R. Langhoff, and D. P. Chong.

16. F. B. Van Duijenveldt, IBM Tech. Res. Rep. RJ947 (no. 16437) (1979).

17. M. J. Frisch, J. A. Pople, and J. S. Binkley, J. Chem. Phys. **80**, 3265 (1984).

18. W. Meyer, P. C. Hariharan, and W. Kutzelnigg, J. Chem. Phys. **73**, 1880 (1980).

19. G. Gioumousis and C. F. Curtiss, J. Math. Phys. **2**, 96 (1961).

20. W. Kołos and L. Wolniewicz, J. Chem. Phys. **43**, 2429 (1965).

21. M. J. Norman, R. O. Watts, and U. Buck, J. Chem. Phys. **81**, 3500 (1984).

22. K. T. Tang, J. M. Norbeck, and P. R. Certain, J. Chem. Phys. **64**, 3063 (1976).

23. F. B. Brown, D. W. Schwenke, and D. G. Truhlar, Theor. Chim. Acta **68**, 23 (1985).

24. B. Liu, J. Chem. Phys. **58**, 1924 (1973); P. Siegbahn and B. Liu, J. Chem. Phys. **68**, 2457 (1978); D. G. Truhlar and C. J. Horowitz, J. Chem. Phys. **68**, 2466 (1978); **71**, 1514 (1979).

25. P. G. Burton and U. E. Senff, J. Chem. Phys. **76**, 6073 (1982).

26. M. Rubinstein and I. Shavitt, J. Chem. Phys. **51**, 2014 (1969).

27. D. M. Silver and R. M. Stevens, J. Chem. Phys. **59**, 3378 (1973).

28. D. G. Truhlar and J. T. Muckerman, in *Atom-Molecule Collision Theory*, ed. by R. B. Bernstein (Plenum Press, New York, 1979), pg. 505.

29. N. C. Blais and D. G. Truhlar, J. Chem. Phys. **65**, 5335 (1976).

30. W. H. Press, B. P. Flannery, S. A. Teukolsky, and W. T. Vetterling, *Numerical Recipes* (Cambridge University Press, Cambridge, 1986), Chapter 7.

31. D. E. Knuth, *Seminumerical Algorithms*, Vol. 2 of *The Art of Computer Programming*, (Addison-Wesley, Reading Mass., 1981), 2nd. edition, Chapter 3.

32. D. L. Bunker and N. C. Blais, J. Chem. Phys. **41**, 2377 (1964).

33. H. Goldstein, *Classical Mechanics* (Addison-Wesley, Reading Mass., 1980), 2nd edition, pg. 344.

34. Reference 30, Chapter 15.

35. R. Bulirsch and J. Stoer, Numer. Math. **8**, 1 (1966).

36. J. P. Rink, J. Chem. Phys. **36**, 262 (1962).

37. R. W. Patch, J. Chem. Phys. **36**, 1919 (1962).

38. E. A. Sutton, J. Chem. Phys. **36**, 2923 (1962).

39. T. A. Jacobs, R. R. Giedt, and N. Cohen, J. Chem. Phys. **47**, 54 (1967).

40. I. R. Hurle, A. Jones, J. L. J. Rosenfeld, Proc. Roy. Soc. **A 310**, 253 (1969).

41. D. O. Ham, D. W. Trainor, and F. Kaufman, J. Chem. Phys. **53**, 4395 (1970).

42. J. W. Duff and D. G. Truhlar, J. Chem. Phys. **63**, 4418 (1975).

43. T. Ashton, D. L. S. McElwain, and H. O. Pritchard, Can. J. Chem. **51**, 237 (1973).

Table I. Parameters for the analytic representation given in Eqs. (1)-(4) of the $^1H_2\,X\,^1\Sigma_g^+$ potential curve. All parameters are in atomic units and are valid only for the isotope of H with mass 1 amu.

r_0	3.5284882	a_6	-1.272679684173909
C_6^a	6.499027	a_7	0.5630423099212294
C_8^a	124.3991	a_8	-0.1879397372273814
C_{10}^a	3285.828	a_9	0.04719891893374140
D	0.160979391	a_{10}	-0.008851622656489644
s	1	a_{11}	0.001224998776243630
a_0	0.03537359271649620	a_{12}	$-1.227820520228028(-4)^b$
a_1	2.013977588700072	a_{13}	$8.638783190083473(-6)$
a_2	-2.827452449964767	a_{14}	$-4.036967926499151(-7)$
a_3	2.713257715593500	a_{15}	$1.123286608335365(-8)$
a_4	-2.792039234205731	a_{16}	$-1.406619156782167(-10)$
a_5	2.166542078766724		

^{a} From Ref. [13].
^{b} The number in parenthesis is the power of ten multiplying the number.

Table II. Computed energies in E_h for separated $H_2 + H_2$.

r_1	r_2	E^{CAS}	E^{MRCI}
1.000	1.401	-2.2501723	-2.2951620
1.401	1.401	-2.3040214	-2.3456759
3.000	1.401	-2.2002567	-2.2286053
5.000	1.401	-2.1548434	-2.1762882
20.00	1.401	-2.1519998	-2.1729908
1.000	1.000	-2.1963232	-2.2446483
20.00	20.00	-1.9999781	-1.9999782

Table III. Computed energies in E_h for linear geometries.

r_1	r_2	R	E^{CAS}	E^{MRCI}
1.000	1.000	3.0	-2.1489968	-2.2021605
1.401	1.000	3.0	-2.1895079	-2.2411766
1.401	1.401	3.0	-2.2277344	-2.2782835
1.000	1.000	3.5	-2.1769510	-2.2280992
1.401	1.000	3.5	-2.2242814	-2.2732647
1.401	1.401	3.5	-2.2708059	-2.3180081
1.000	1.000	4.0	-2.1885540	-2.2384542
1.401	1.000	4.0	-2.2392485	-2.2864936
1.401	1.401	4.0	-2.2894001	-2.3342640
1.000	1.000	4.5	-2.1932777	-2.2424759
1.000	1.401	4.5	-2.2456559	-2.2918954
1.401	1.000	4.5	-2.2456556	-2.2918956
1.401	1.401	4.5	-2.2976739	-2.3411200
3.000	1.401	4.5	-2.1810055	-2.2164670
5.000	1.401	4.5	-2.0795631	-2.1188059
1.000	1.000	5.0	-2.1951517	-2.2439630
1.401	1.000	5.0	-2.2483393	-2.2940230
1.401	1.401	5.0	-2.3013097	-2.3439591

Table IV. Computed energies in E_h for T shaped geometries.

r_1	r_2	R	E^{CAS}	E^{MRCI}
1.000	1.000	3.0	−2.1581148	−2.2109995
1.000	1.401	3.0	−2.2026122	−2.2541250
1.401	1.000	3.0	−2.2083495	−2.2584915
1.401	1.401	3.0	−2.2534653	−2.3025120
1.000	1.000	3.5	−2.1806088	−2.2315200
1.000	1.401	3.5	−2.2294472	−2.2781860
1.401	1.000	3.5	−2.2322244	−2.2802336
1.401	1.401	3.5	−2.2811433	−2.3271734
3.000	1.401	3.5	−2.1774572	−2.2105028
5.000	1.401	3.5	−2.1459055	−2.1699190
1.000	1.000	4.0	−2.1900624	−2.2398409
1.000	1.401	4.0	−2.2414512	−2.2885466
1.401	1.000	4.0	−2.2427205	−2.2894577
1.401	1.401	4.0	−2.2940422	−2.3382245
1.401	3.000	4.0	−2.1715427	−2.2091528
3.000	1.401	4.0	−2.1892140	−2.2205532
1.401	5.000	4.0	−2.0467742	−2.0870823
5.000	1.401	4.0	−2.1500841	−2.1731692
1.000	1.000	4.5	−2.1939053	−2.2430450
1.000	1.401	4.5	−2.2466281	−2.2927943
1.401	1.000	4.5	−2.2471777	−2.2931716
1.401	1.401	4.5	−2.2998260	−2.3429269
1.000	1.000	5.0	−2.1954200	−2.2442018
1.000	1.401	5.0	−2.2487844	−2.2944316
1.401	1.000	5.0	−2.2490111	−2.2945755
1.401	1.401	5.0	−2.3023270	−2.3448057

Table V. Computed energies in E_h for parallel shaped geometries.

r_1	r_2	R	E^{CAS}	E^{MRCI}
1.000	1.000	3.00	−2.1630376	−2.2141120
1.401	1.000	3.00	−2.2125055	−2.2605994
1.401	1.401	3.00	−2.2614119	−2.3065803
1.401	1.401	3.00	−2.2468856	−2.3062874
1.000	1.000	3.50	−2.1827285	−2.2326254
1.401	1.000	3.50	−2.2340995	−2.2809217
1.401	1.401	3.50	−2.2851299	−2.3289184
1.000	1.401	3.75	−2.2397741	−2.2861676
1.401	1.401	3.75	−2.2915579	−2.3348676
3.000	1.401	3.75	−2.1853072	−2.2155281
5.000	1.401	3.75	−2.1486507	−2.1716260
1.000	1.000	4.00	−2.1909127	−2.2401360
1.401	1.000	4.00	−2.2434838	−2.2895480
1.401	1.401	4.00	−2.2958436	−2.3387790
1.000	1.000	4.50	−2.1942165	−2.2430549
1.401	1.000	4.50	−2.2474464	−2.2930622
1.401	1.401	4.50	−2.3005503	−2.3429644
1.000	1.000	5.00	−2.1955172	−2.2441340
1.401	1.000	5.00	−2.2490789	−2.2944289
1.401	1.401	5.00	−2.3025690	−2.3446655

Table VI. Computed energies in E_h for cross shaped geometries.

r_1	r_2	R	E^{CAS}	E^{MRCI}
1.401	1.401	2.00	−2.1169936	−2.1692110
1.000	1.000	3.00	−2.1631831	−2.2146856
1.401	1.000	3.00	−2.2129581	−2.2615710
1.401	1.401	3.00	−2.2624792	−2.3082718
1.000	1.000	3.50	−2.1827569	−2.2328906
1.401	1.000	3.50	−2.2342374	−2.2813539
1.401	1.401	3.50	−2.2854980	−2.3296479
1.000	1.401	3.75	−2.2398544	−2.2864620
1.401	1.401	3.75	−2.2917836	−2.3353583
3.000	1.401	3.75	−2.1861503	−2.2165969
5.000	1.401	3.75	−2.1491633	−2.1719592
1.000	1.000	4.00	−2.1909183	−2.2402610
1.401	1.000	4.00	−2.2435329	−2.2897484
1.401	1.401	4.00	−2.2959868	−2.3391111
1.000	1.000	4.50	−2.1942185	−2.2431111
1.401	1.000	4.50	−2.2474683	−2.2931541
1.401	1.401	4.50	−2.3006153	−2.3431180
1.000	1.000	5.00	−2.1955189	−2.2441593
1.401	1.000	5.00	−2.2490912	−2.2944721
1.401	1.401	5.00	−2.3026036	−2.3447394
1.401	1.401	6.00	−2.3037829	−2.3455943

Table VII. Parameters for the analytic representation of the interaction potential. All parameters are in atomic units.

a_Q	0.685147	m_8^2	3
b_Q	-0.198019	$\tilde{a}_8^2$	0.196784
c_Q	0.144382	$\tilde{b}_8^2$	0.508106
d_Q	0.449685	d_1^{LR}	54
m_6^0	1	d_2^{LR}	0.4
$\tilde{a}_6^0$	1.17467	A_p	0.717277143
$\tilde{b}_6^0$	1.72657	B_p	1.00471655
m_6^2	2	C_p	1.27158465
$\tilde{a}_6^2$	0.0198867	$^3\alpha$	7
$\tilde{b}_6^2$	0.0681996	β	0.1
m_8^0	2	ρ_o	11
$\tilde{a}_8^0$	9.52859	a^D	2
$\tilde{b}_8^0$	0.796373	r^D	5.4
		β^A	20

Table VIII. Parameters for the multiplicative correction factor of Eq. (17)[a]. All parameters are in atomic units.

ijk	c_{000}^{ijk}	c_{200}^{ijk}	c_{220}^{ijk}	c_{222}^{ijk}
0 0 0	$8.2335075(-1)$[b]	$9.4069522(-2)$	$7.9142831(-3)$	$-4.7369816(-3)$
0 1 0	$1.9927182(-1)$	$-2.6657323(-2)$	$-8.7591868(-3)$	$9.4419462(-3)$
1 0 0	$1.9927182(-1)$	$-1.7873925(-1)$	$-8.7591868(-3)$	$9.4419462(-3)$
1 1 0	$-2.7306801(-1)$	$7.6910059(-2)$	$5.4783229(-3)$	$-1.6362036(-2)$
0 0 1	$-2.1105535(-1)$	$-1.7750047(-2)$	$4.5662762(-4)$	$5.3064904(-4)$
0 1 1	$8.1872059(-3)$	$1.6826832(-2)$	$-2.4577906(-3)$	$-1.7568388(-3)$
1 0 1	$8.1872059(-3)$	$3.7743965(-2)$	$-2.4577906(-3)$	$-1.7568388(-3)$
1 1 1	$8.1615668(-2)$	$-3.8437296(-2)$	$8.2469313(-3)$	$4.0949053(-3)$

[a] $c_{020}^{ijk} = c_{200}^{jik}$.
[b] The number in parenthesis is the power of ten multiplying the number.

Table IX. Three body recombination rate constants.

$T(K)$	k^{3B} $(10^{14}\ cm^6 mol^{-2} sec^{-1})$
100	$18.4 \pm 4.5\%$[a]
300	$15.2 \pm 5.4\%$
1000	$9.82 \pm 5.4\%$
2000	$6.81 \pm 6.2\%$
3000	$4.87 \pm 6.6\%$
5000	$3.31 \pm 6.9\%$

[a] One sigma error bars.

Figure Captions.

Fig. (1): Effective Morse exponent α and r times α as a function of r for the H_2 potential.

Fig. (2): The $H_2 + H_2$ interaction potential for $R = 4$, $r_1 = 1.4\ a_o$, $\theta_1 = \phi = 0$, $\theta_2 = \pi/2$ as a function of r_2 for various stages of the fit.

Fig. (3): Angular expansion coefficients $v_{q_1 q_2 \mu}$ of the interaction potential as a function of R. The bond lengths are $1.449\ a_o$. The DHR potential is from Ref. [7] and the PNO-CI and CEPA2 results are from Ref. [25].

Fig. (4): A comparison of the relative errors obtained using the Burlisch-Stoer (B.S.) algorithm and the Adams-Bashforth-Moulton (A.B.M.) algorithm as a function of CPU time.

Fig. (5): A comparison of the theoretical and experimental recombination rate constants.

Fig. (6): A comparison of the results using the potential of Sect. II and the results obtained using the DHR potential of Ref. [7] with the estimate of the recombination rate based on experiment [1].

H2 "MORSE" EXPONENT
FOR AD POTENTIAL

$$\frac{\alpha}{r\alpha}$$

figure 1.

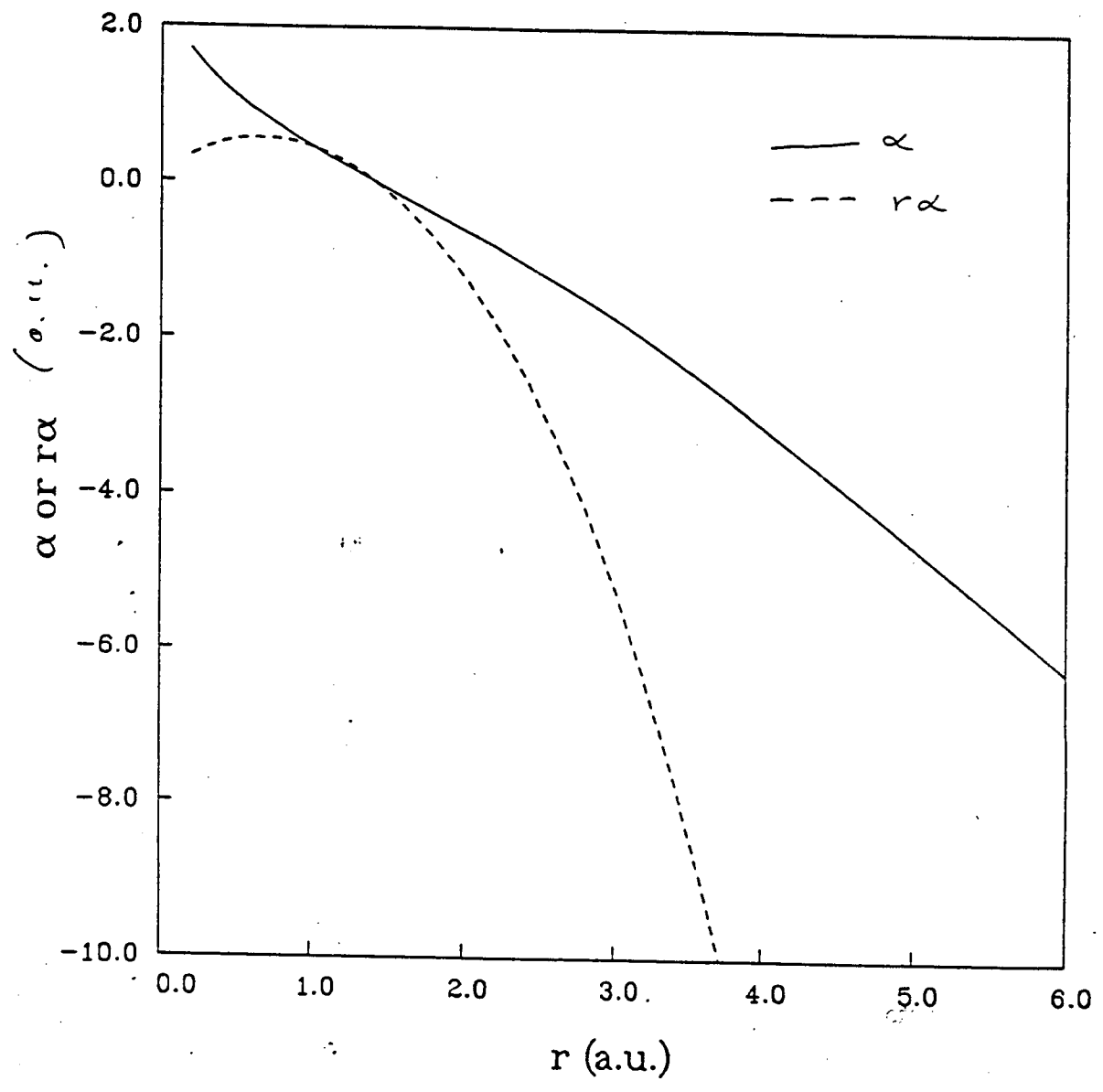H2+H2 POTENTIAL CUTS
R=4,1.4,0,90,0

+ MRCI
.... LONDON
--- PAIR
--- FIT
— LSTH
— SCALED LSTH

+ V^{MRCI}

.... $\tilde{V}_{H_4}^{Lon}$

-- V_{H_4}

-- V^{LD}

-- $V_{ASH?D}^{ScaLD}$

— V

Fig 3

Comparing WMR and present potential
first angular components, r1=r2=1.4

present 000	present, 6 angles 020
present 020	□ PNOCl
WMR 000	O CEPA2
WMR 020	△ PNOCl 020
present, 6 angles 000	+ CEPA2 020

Legend on plot:
- V_{000} accurate
- V_{200} accurate
- V_{000} 6 angle
- V_{200} 6 angle
- V_{000} DHR
- V_{200} DHR
- □ V_{000} PNO-CI
- △ V_{200} PNO-CI
- O V_{000} CEPA2
- + V_{200} CEPA2

x-axis: R (ao)

y-axis: $V_{\beta_1\beta_2\mu}$ (r,E_h)

fig. 4

Error of various integrators
BS vs. ABM

Fig. 5

Figure 5. Semi-logarithmic plot of rate coefficient versus temperature T (K), with axes $\log(k \; cm^6 mol^{-2} sec^{-1})$ and $\log(k \; cm^3 mol^{-1} sec^{-1})$.

Fig. 9